Biochemical and Biophysical Research Communications 422 (2012) 745–750

Contents lists available at SciVerse ScienceDirect

Biochemical and Biophysical Research Communications

journal homepage: www.elsevier.com/locate/ybbrc

Crystal structure of *Helicobacter pylori* neutrophil-activating protein with a di-nuclear ferroxidase center in a zinc or cadmium-bound form

Hideshi Yokoyama *, Osamu Tsuruta, Naoya Akao, Satoshi Fujii

School of Pharmaceutical Sciences, University of Shizuoka, 52-1 Yada, Suruga-ku, Shizuoka 422-8526, Japan

ARTICLE INFO

Article history:
Received 8 May 2012
Available online 19 May 2012

Keywords:
Helicobacter pylori
Neutrophil-activating protein
Zinc
Cadmium
Dps
Ferroxidase center

ABSTRACT

Helicobacter pylori neutrophil-activating protein (HP-NAP) is a Dps-like iron storage protein forming a dodecameric shell, and promotes adhesion of neutrophils to endothelial cells. The crystal structure of HP-NAP in a Zn^{2+}- or Cd^{2+}-bound form reveals the binding of two zinc or two cadmium ions and their bridged water molecule at the ferroxidase center (FOC). The two zinc ions are coordinated in a tetrahedral manner to the conserved residues among HP-NAP and Dps proteins. The two cadmium ions are coordinated in a trigonal–bipyramidal and distorted octahedral manner. In both structures, the second ion is more weakly coordinated than the first. Another zinc ion is found inside of the negatively-charged threefold-related pore, which is suitable for metal ions to pass through.

1. Introduction

Helicobacter pylori, a Gram-negative bacterium, chronically infects up to 50% of the world's human population, and causes severe diseases such as chronic gastritis, peptic ulcers, and stomach cancers. *H. pylori*-induced gastritis is typically associated with infiltration of the infected stomach mucosa by neutrophils [1,2]. Among a number of virulence factors, *H. pylori* neutrophil-activating protein (HP-NAP) attracts and activates neutrophils, and promotes adhesion of neutrophils to endothelial cells. The protein also induces the production of reactive oxygen radicals by activating the NADPH oxidase [3,4]. HP-NAP is a major antigen in the immune response to *H. pylori* infections, and is a candidate for an anti-*H. pylori* vaccine [4,5].

The crystal structure of HP-NAP from *H. pylori* strain 26695 (HP-NAP 26695) was the first to be determined [6]. HP-NAP is a dodecameric protein consisting of 17-kDa monomers with a central cavity where iron ions bind. HP-NAP can bind up to 500 atoms of iron per dodecamer in vitro [7]. The amino acid sequence and overall structure of HP-NAP are similar to those of bacterial ferritins [8] and Dps (DNA-protecting proteins under starved conditions) proteins [9] (Fig. S1). Ferritin detoxifies and stores iron ions by sequestering them. Ferritin binds metals such as Cd^{2+}, Zn^{2+}, Tb^{3+}, or Ca^{2+} in addition to Fe^{2+} [10]. Given its structural similarity with ferritin, HP-NAP may bind metals other than iron, although, to our knowledge, there are no such reports. HP-NAP protects *H. pylori* from iron-mediated oxidative DNA damage by sequestering free iron [11], similar to Dps proteins which protect DNA from oxidative damage [12].

Recently, we determined the native form and an iron-containing form of HP-NAP from strain YS39 (HP-NAP YS39 apo and YS39 Fe, respectively) [13]. The amino-acid sequence of HP-NAP YS39 is similar to that of HP-NAP 26695 as shown in Fig. S1. HP-NAP YS39 differs from HP-NAP 26695 at four residues (E46G, V59A, I73L, and Y101H). Another strain, HP-NAP YS29 differs from HP-NAP 26695 at one residue (Y101H). Among HP-NAPs and DPS proteins, His25, His37, Asp52, and Glu56 are completely conserved, and involved in metal-binding at the FOC as described [13]. In order to understand the metal storage function of HP-NAP, we determined the crystal structures of Zn^{2+}- and Cd^{2+}-bound forms of YS39 (YS39 Zn and YS39 Cd, respectively), and Cd^{2+}-bound and apo forms of YS29 (YS29 Cd and YS29 apo, respectively). By comparing the structures determined here and previously [13], we will discuss the difference in metal-coordination between the Fe^{3+}-, Zn^{2+}- and Cd^{2+}-bound forms, and the structure of the pores which metal ions pass through.

2. Materials and methods

2.1. Protein expression, purification, and crystallization

HP-NAP YS39 and YS29 were prepared as described previously [13]. Crystallization was carried out with the hanging-drop (for

Abbreviations: HP-NAP, *Helicobacter pylori* neutrophil-activating protein; FOC, ferroxidase center.

* Corresponding author. Fax: +81 54 264 5641.
E-mail address: h-yokoya@u-shizuoka-ken.ac.jp (H. Yokoyama).

0006-291X/$ - see front matter © 2012 Elsevier Inc. All rights reserved.
http://dx.doi.org/10.1016/j.bbrc.2012.05.073

YS39 Zn) or sitting-drop (for the others) vapor-diffusion method at 20 °C. Crystallization drops were prepared by mixing 0.5 μl of protein solution and 0.5 μl of reservoir solution. The protein solution was 10–15 mg/mL in 50 mM Tris–HCl and 0.1 M L-arginine (pH 8.8). Crystals of YS39 Cd and YS29 Cd were prepared using a reservoir solution containing 50 mM $CdSO_4$, 1.0 M sodium acetate, and 0.1 M HEPES–NaOH (pH 7.5), and crystals of YS29 apo were prepared using a reservoir solution containing 2.0 M ammonium sulfate and 0.1 M Tris–HCl (pH 7.5). Crystals of cubic or rectangular form appeared and grew to an approximate size of 0.2 mm per side. To obtain crystals of YS39 Zn, a reservoir solution containing 20% (v/v) ethylene glycol was used, and the resultant crystals were soaked in a solution containing 20% (v/v) ethylene glycol and 20 mM $ZnSO_4$ for 15 min.

2.2. Data collection and refinement

Crystals were transferred into a solution of 30% (v/v) glycerol in the mother liquor in case of YS39 Zn, YS39 Cd, and YS29 Cd, and 20% (v/v) glycerol in the mother liquor in case of YS29 apo, and were flash-frozen in a stream of N_2 at 95 K. For YS39 Cd, X-ray diffraction data were collected on a Rigaku R-AXIS IV++ image-plate area detector, equipped with a Rigaku ultraX 18 rotating-anode X-ray generator operated at 50 kV and 200 mA, and were processed and scaled with d*TREK [14]. The X-ray diffraction data for the others were collected at beamlines NW12A and BL6A at the KEK Photon Factory (Tsukuba, Japan), and processed and scaled with HKL2000 [15].

Structures were solved by the molecular replacement method using MOLREP [16] in the CCP4 suite [17] with chain A of HP-NAP YS39 Fe (Protein Data Bank (PDB) code 3TA8) [13] as a search model. Crystallographic refinements were made with REFMAC5 [18] in the CCP4 suite. Model building and structural adjustments were performed with COOT [19]. An anomalous difference map was calculated using the data collected at 1.2820 Å for YS39 Zn. Notable anomalous difference peaks were observed at the known FOC, the inside of pore I (Fig. 1), and other sites. In YS39 Cd and YS29 Cd, notable $F_o - F_c$ electron densities over 10σ were observed if cadmium ions were omitted from the structures (Fig. S2). Fluorescence scanning around the Fe K-absorption edge (1.7409 Å) using crystals of YS39 Cd and YS29 Cd revealed no peaks. The structure does not contain iron atoms, and thus the electron densities over 10σ were assigned to cadmium ions. Data collection and refinement statistics are summarized in Table 1. According to the stereochemistry of the model evaluated with RAMPAGE [20], no residues are located in the outlier region. All molecular figures were produced with PyMOL (http://pymol.sourceforge.net/). The least squares fittings between two structures were performed with PDBeFold [21] or LSQKAB in the CCP4 suite.

2.3. RCSB Protein Data Bank accession numbers

Atomic coordinates and structure factors have been deposited in the RCSB Protein Data Bank with the accession codes 4evb (HP-NAP YS39 Zn), 4evc (YS39 Cd), 4evd (YS29 Cd), and 4eve (YS29 apo).

3. Results and discussion

3.1. Overall structure of the dodecamer

All the crystals in this study belong to the cubic space group *F*432 with one monomer in the asymmetric unit which is the same as those of YS39 Fe and YS39 apo [13]. A total of 12 protomers form a dodecamer like a spherical shell about 90 Å in diameter with crystallographic point group 23 (Fig. 1). The internal cavity of the dodecamer is about 50 Å in diameter. The overall structure of HP-NAP YS39 is similar to those of other HP-NAPs and Dps proteins. According to the superposition of the Cα atoms based on the protomer of HP-NAP YS39 Zn, the root-mean-square differences (r.m.s.d.s) are 0.26 Å (YS39 Cd), 0.31 Å (YS39 Fe) [13], 0.59 Å (YS39 apo) [13], and 0.30 Å (HP-NAP 26695) [6]. The r.m.s.d.s are 0.91 Å (*Listeria innocua* ferritin) [8], 1.77 Å (*Escherichia coli* Dps) [9], and 1.76 Å (*Salmonella enterica* Dps) [22]. Although DPS proteins have a 26-residue longer N-terminal end than HP-NAP Y39, each DPS protomer was relatively similar to HP-NAP YS39 (Fig. S1).

The cell dimension of YS39 Zn (a = 185.53 Å) is about 4 Å shorter than that of YS39 apo (a = 189.47 Å) [13], although inter-dodecamer contacts made through the bridged stacks of Lys74 residues [13] show no difference: distances between two Lys74 Cα atoms from adjacent subunits are 4.4 Å for YS39 Zn and 4.5 Å for YS39 apo. Therefore, the YS39 Zn dodecamer is smaller in diameter than YS39 apo. The approximate volume of the internal cavity as calculated by CASTp [23] is 7.0×10^4 Å^3 for YS39 Zn, 20% smaller than that for YS39 apo (8.8×10^4 Å^3). The volume of *S. enterica* Dps is 5.3×10^4 Å^3, much smaller than that for YS39 Zn, although their protomers are similar to each other.

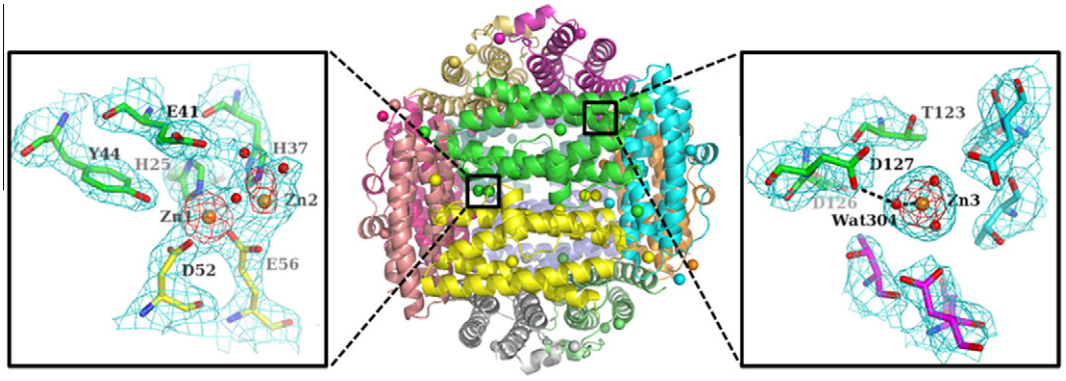

Fig. 1. Overall structure of HP-NAP YS39 Zn with a close-up view of the di-zinc FOC (left inset) and threefold-related pore I (right inset). Each subunit with zinc ions is shown in a different color. Each inset provides a view from the inner side of the dodecamer. The $2F_o - F_c$ electron density maps (cyan) are contoured at the 1.0σ level, and the anomalous difference maps around zinc ions (red) are contoured at the 8σ level. In the insets, zinc ions and water molecules are depicted as orange and red spheres, respectively. Dotted lines indicate interactions around Zn3. (For interpretation of the references to color in this figure legend, the reader is referred to the web version of this article.)

Table 1
Data collection and refinement statistics.

	YS39 Zn		YS39 Cd	YS29 Cd	YS29 apo
Data collection					
Space group	*F*432		*F*432	*F*432	*F*432
Cell dimensions (Å)	*a* = 185.53		*a* = 186.71	*a* = 187.41	*a* = 187.79
Wavelength (Å)	1.2892	1.2820	1.5418	0.9780	0.9780
Resolution range (Å)	50.0–2.5 (2.54–2.50)[a]	50.0–2.5 (2.54–2.50)	56.3–2.4 (2.49–2.40)	20.0–2.2 (2.28–2.20)	20.0–2.1 (2.17–2.10)
R_{merge} (I)[b]	0.046 (0.371)	0.051 (0.492)	0.099 (0.288)	0.080 (0.383)	0.054 (0.301)
Average $I/\sigma I$	63.6 (9.4)	58.7 (7.2)	10.1 (5.0)	38.1 (8.2)	44.1 (9.2)
Total reflections	133,480	134,051	78,025	153,455	163,638
Unique reflections	9990	9953	11,426	14,790	16,933
Completeness (%)	99.2 (100.0)	99.5 (100.0)	99.9 (100.0)	99.4 (99.6)	98.7 (97.4)
Refinement					
Resolution range (Å)	20.00–2.50		20.00–2.40	19.65–2.20	19.69–2.10
No. of reflections used	8819		10,276	13,236	15,121
Completeness (%)	98.5		100.0	99.3	98.2
R_{work}[c]/R_{free}[d]	0.227/0.291		0.219/0.250	0.213/0.237	0.216/0.252
No. of atoms per subunit					
Protein	1179		1179	1186	1194
Solvent	85		71	85	132
Metal ion	Zn^{2+} × 7		Cd^{2+} × 13	Cd^{2+} × 16	0
Average *B*-factor (Å^2)	50.4		26.5	24.2	23.2
R.m.s. deviations					
Bond lengths (Å)	0.014		0.008	0.007	0.006
Bond angles (°)	1.471		1.015	0.961	0.947
Ramachandran plot[e] *(%)*					
Favored region	100.0		100.0	99.3	100.0
Allowed region	0		0	0.7	0
Outlier region	0		0	0	0

[a] Values in parentheses are for the highest-resolution shell.
[b] R_{merge} (I) = $\Sigma|I - \langle I\rangle|/\Sigma I$, where I is observed diffraction intensity.
[c] $R = \Sigma||F_o| - |F_c||/\Sigma|F_o|$, where F_o and F_c are observed and calculated structure amplitudes, respectively.
[d] R_{free} is an R value for 10% of reflections chosen randomly and omitted from refinement.
[e] Values were calculated with RAMPAGE [20].

3.2. Ferroxidase center in the zinc-bound or cadmium-bound form

In YS39 Zn, two zinc ions are located at the FOC between two protomers (Fig. 1). The peak heights of anomalous difference maps were 29σ (Zn1) and 14σ (Zn2). As shown in Fig. 2A, the Zn1 ion is coordinated in a tetrahedral manner to His25 Nε2, Asp52 Oδ2, Glu56 Oε1, and a water molecule bridging two zinc ions (The coordination distances are shown in Table 2). The Zn2 ion is coordinated in a distorted tetrahedral manner to His37 Nε2, Glu56 Oε2, and two water molecules. His25 and His37 are located on helices 1 and 2 of one subunit, respectively, and both Asp52 and Glu56 are located on helix 2 of the other subunit (Fig. 2 and Fig. S1). In the FOC of YS39 Fe, a ferric ion is located at almost the same position as Zn1, and is in a similar coordination as YS39 Zn except for the absence of a bridged water molecule and longer metal–ligand distances (Table 2), whereas no atom occupies the Zn2 position (Fig. 2A). In HP-NAP 26695 [6], a ferric iron is located at almost the same position as Zn1, and an unidentified solvent ion is located at a similar position to Zn2.

In YS39 Cd, two cadmium ions are located at the FOC similarly as in YS 39 Zn (Fig. 2B and Fig. S2A). The peak heights of $F_o - F_c$ omit maps with phases from a model without Cd1 and Cd2 were 42σ (Cd1) and 25σ (Cd2). The Cd1 ion is coordinated in a trigonal–bipyramidal manner, where the triangle is formed by His25 Nε2, Asp52 Oδ2, and a water molecule bridging two cadmium ions, and the corner of the pyramid is formed by Glu56 Oε1 and another water molecule. The Cd2 ion is coordinated in a distorted octahedral manner to His37 Nε2 and three water molecules, with two sites not occupied. Cadmium cations tend to coordinate in both tetrahedral and octahedral arrangements, but are known to exhibit a versatile coordination geometry, whereas zinc cations tend to coordinate in a tetrahedral arrangement [24]. In the case of the binuclear cadmium center of phosphotriesterase, one cadmium ion is coordinated in a trigonal–bipyramidal manner [25].

The average coordination distance between Zn1 and its ligands is 2.13 Å, whereas that between Zn2 and its ligands is longer, 2.41 Å (Table 2). The *B*-factor for Zn1 is 48.8 Å^2, lower than for Zn2, 51.9 Å^2. The average coordination distance between Cd1 and its ligands is 2.38 Å, whereas that between Cd2 and its ligands is longer, 2.62 Å. The *B*-factor for Cd1 is 20.6 Å^2, lower than for Cd2, 42.1 Å^2. According to these results, in both YS39 Zn and YS39 Cd, the second coordination is weaker than the first. In a di-iron FOC of *Bacillus brevis* Dps, the second iron exhibits a loose coordination [26]. As described in Haikarainen et al. [27], the second ion site in the FOC is only transiently occupied. It is possible that the di-iron sites are occupied only by Fe^{2+}, which is rapidly oxidized to Fe^{3+} [28]. Therefore, in crystals of YS39 Fe following long exposure to oxygen, there is no second ion in the FOC [13].

In the FOC of YS39 Zn, two zinc ions are separated by a distance of 3.3 Å, which is similar to the di-zinc distance in the FOC of two Dps-like proteins, *Streptococcus pyogenes* Dpr (3.5 Å) [27] and *S. suis* Dpr (3.3 Å) [29]. In the FOC of YS39 Cd and YS29 Cd, two cadmium ions are separated by 4.2 and 4.3 Å, respectively, longer than the di-zinc distance of YS39 Zn. The mean metal–ligand bond distance (in the case of His, Asp, and Glu) in metalloproteins is 2.14 Å for Zn^{2+} and 2.39 Å for Cd^{2+} [24]. These distances are comparable to values for Zn1 (YS39 Zn) and Cd1 (YS39 Cd) (Table 2). Because of the longer metal–ligand distance for Cd^{2+}, the Cd2 of YS39 Cd is located 1.3 Å from the Zn2 position of YS39 Zn (Fig. 2B), resulting in a longer Cd1–Cd2 distance.

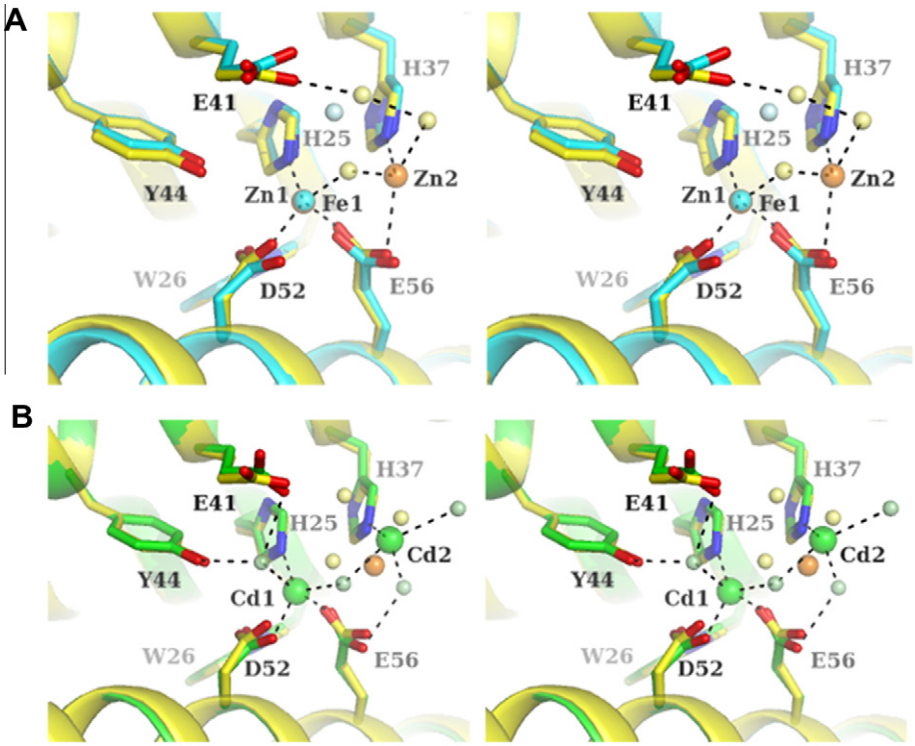

Fig. 2. Comparison of HP-NAP ferroxidase centers in a stereo representation. Zinc ions and water molecules in YS39 Zn are colored in orange and pale yellow, respectively. Metal ions and water molecules in the other structures are shown in the same color as described below. Dotted lines indicate interactions for YS39 Zn (A) and YS39 Cd (B). (A) Superposition of YS39 Zn (yellow) and YS39 Fe (cyan) [13] (r.m.s.d. 0.39 Å of two subunits). (B) Superposition of YS39 Zn (yellow) and YS39 Cd (green) (r.m.s.d. 0.33 Å). (For interpretation of the references to color in this figure legend, the reader is referred to the web version of this article.)

Table 2
Metal–ligand distances of the FOC in HP-NAP YS39. Values are in Å (*B*-factors, in Å^2). The values for YS39 Fe are from [13].

	YS39 Zn	YS39 Cd	YS39 Fe
Zn1/Cd1/Fe1 (B_{factor})	48.8	20.6	40.2
His25 Nε2	2.01	2.32	2.47
Asp52 Oδ2	1.98	2.24	2.37
Glu56 Oε1	2.08	2.29	2.15
HOH1	2.46	2.52	–
HOH2	–	2.54	–
Average distance	2.13	2.38	2.33
Zn2/Cd2/– (B_{factor})	51.9	42.1	–
His37 Nε2	2.20	2.55	–
Glu56 Oε2	2.80	–	–
HOH1	2.03	2.56	–
HOH3	2.61	2.43	–
HOH4	–	2.93	–
Average distance	2.41	2.62	–

3.3. Threefold channel pore

The HP-NAP dodecamer contains two types of threefold-related pores; pore I and pore II (designated as N-terminal and C-terminal pores in Dps, respectively) [13]. Pore I has a strong hydrophilic and negatively charged environment that might encourage metal-ion entry into the protein, and has three layers of negatively charged residues, Glu114, Asp126, and Asp127 (from outside to inside), as shown in Fig. 3. These residues are conserved among HP-NAPs, but not in the Dps proteins (Fig. S1). The positively charged residue, Lys115, is positioned outside the entrance to the pore, and may function as an electrostatic guide for metal-ion transfer. Inside of pore I of YS39 Zn (Fig. 1), a zinc ion (Zn3) with an anomalous difference peak (17σ) is coordinated to three symmetrically-related water molecules (Wat304 with 0.33 occupancy) at a distance of 2.0 Å, each of which is hydrogen-bonded to the Asp127 Oδ1 (distance of 2.9 Å). The Fe2 ion in YS39 Fe is located at almost the same position as Zn3 in YS39 Zn (Fig. 3B), whereas cadmium ions are not observed around pore I in YS39 Cd. Outside of pore I (Fig. 3A), one of three symmetrically-related water molecules (Wat344 with 0.33 occupancy) is hydrogen-bonded to Glu114 Oε2 (2.6 Å) and Lys119 Nζ (2.8 Å). In YS39 Fe, on the other hand, Lys119 Nζ is not located around the center of the threefold pore, but is hydrogen-bonded to the Asn111 Oδ1 of the adjacent subunit (2.6 Å), as is the case in YS39 Cd. In YS39 Zn, the pore path, distance between Wat304 and Wat344, is 12.6 Å (Fig. 3B). The intersubunit distances between two corresponding atoms of the three protomers are as follows; Glu114 Oε2 (5.4 Å), Lys119 Nζ (4.5 Å), Asp126 Oδ2 (8.1 Å), and Asp127 Oδ1 (6.9 Å). The flexible side-chain of Lys119 forming the narrow pore may function as a filter bulb to desolvate hydrated metal ions.

The height of *B*-factors of the threefold-related trimer around pore I is shown in Fig. 4. Each crystal contains 20 mM Zn^{2+} (YS39 Zn), 50 mM Cd^{2+} (YS39 Cd), 5 mM Fe^{3+} (YS39 Fe), and no metal ion (YS 39 apo). In YS39 Zn and YS39 Cd, the central loops around pore I show relatively high *B*-factors. In YS39 Fe, the central and peripheral loops of the trimer show high *B*-factors. In YS39 apo, on the other hand, the central loops show relatively low *B*-factors. Clearly, the apo and metal-bound forms differ in mobility around the pores. At a high concentration of metal ions, the ions and water molecules may frequently enter and exit pore I. According to these observations, pore I is suitable for the metal ions to pass through. While, at the other threefold-related pore (pore II) composed of Thr31, Asp32, and Asn35, no metal ions were observed in YS39 Zn, YS39 Cd, and YS39 Fe.

3.4. Other metal-binding sites

Inside the dodecamer of YS39 Zn, another zinc-binding site is found. The Zn7 ion is 9.3 Å from Zn1, and interacts with the

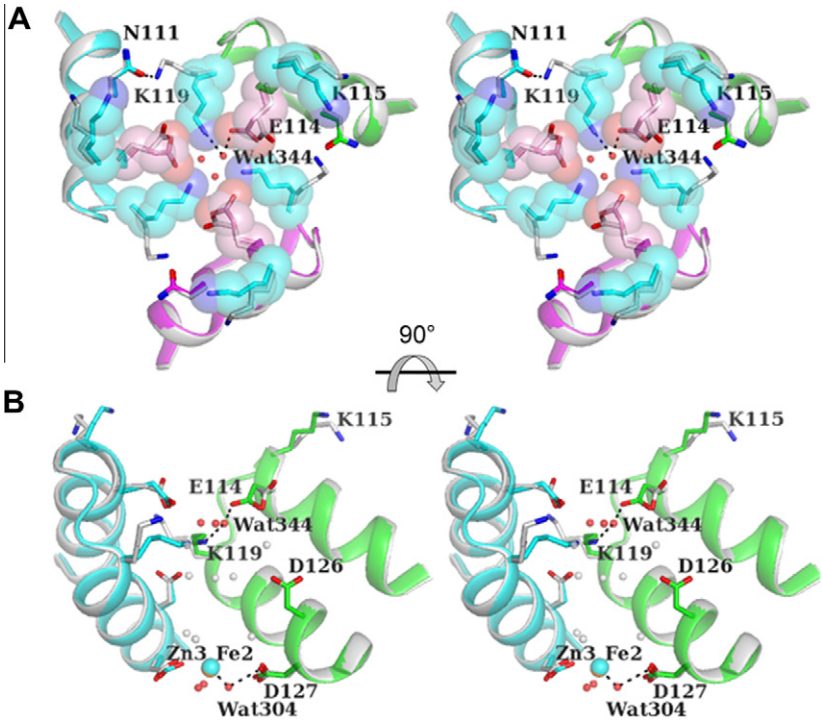

Fig. 3. Comparison of pore I along threefold axes in a stereo representation. Superposition of the threefold-related trimers of YS39 Zn (green, cyan, and magenta) and YS39 Fe (gray) [13]. Zinc ions and water molecules in YS39 Zn are colored in orange and red, respectively. Iron ions and water molecules in YS39 Fe are in cyan and gray, respectively. (A) The view is opposite to the right inset of Fig. 1 (from outside of the spherical shell). Key residues forming pore I are shown with sticks. Acidic and basic residues in YS39 Zn are also represented by pink and cyan space-filling models, respectively. Dotted lines indicate interactions for YS39 Zn and YS39 Fe. (B) Side view of pore I. One polypeptide chain is omitted for clarity. (For interpretation of the references to color in this figure legend, the reader is referred to the web version of this article.)

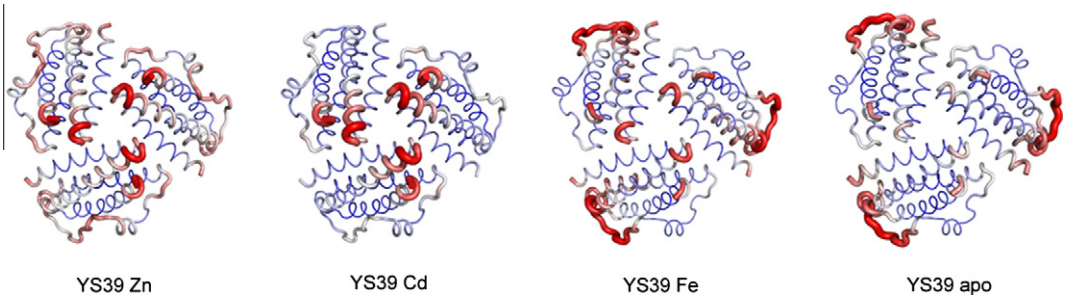

Fig. 4. Thermal motion of trimers along pore I viewed from the outer surface. The *B*-factor scale of main-chain atoms for each residue is shown by the width and color of the tubes. Red thick tubes indicate high *B*-factors, and white thin tubes indicate low *B*-factors. *B*-factors are as follows; YS39 Zn (average 48.6 Å^2, minimum 37.3 Å^2, maximum 64.1 Å^2), YS39 Cd (average 25.6 Å^2, minimum 19.2 Å^2, maximum 38.8 Å^2), YS39 Fe (average 39.2 Å^2, minimum 25.3 Å, maximum 57.5 Å), and YS39 apo (average 34.7 Å^2, minimum 24.6 Å^2, maximum 52.4 Å^2).

side-chains of Glu41 and Glu45 (Fig. S3A). In the YS39 Cd, the Cd8 ion is located at almost the same place as Zn7 of YS39Zn, and interacts with the side-chains of Glu42 and Glu45 (Fig. S3B). The Cd5 ion is 8.2 Å from Cd1 of the other twofold-related subunit, and interacts with the side-chains of Glu49 and Asp53. HP-NAP can bind up to 500 iron ions per dodecamer [7]. Thus metal-binding sites around Zn7, Cd5, and Cd8 are involved in the metal-storage function. In YS39 Zn, four zinc ions per subunit (Zn1, 2, 3, and 7) (Fig. S3A and Fig. 1) are located inside of the dodecamer. The other three zinc ions (Zn4, 5, and 6) are located outside. Their ligands are mostly His residues (Fig. S1). In YS39 Cd, four cadmium ions per subunit (Cd1, 2, 5, and 8) (Fig. S3B) are located inside of the dodecamer, and the other nine cadmium ions are located outside. The binding of many Cd^{2+} ions to the protein is due to the high concentration of Cd^{2+} (50 mM) in the YS39 Cd crystal.

3.5. Structure of another strain YS29

HP-NAP YS39 differs from YS29 at three residues (E46G, V59A, and I73L) as shown in Fig. S1. In YS29 Cd, two cadmium ions are located at the FOC, as in YS39 Cd (Fig. S2B). In overall structure and cadmium-binding sites, no major differences between YS29 and YS39 are observed. One minor difference is that YS29 Cd contains an additional cadmium ion which is weakly coordinated to the Glu46 side-chain (Fig. S3B and C).

The binding of cadmium ions to YS29 apo leads to similar conformational changes in the FOC as does the binding of iron irons in YS39 [13]. Between YS29 Cd and YS29 apo, His25, His37, Glu41, and Tyr44 residues are well superposed (Fig. S4). In comparison with YS29 apo, the side chains of Asp52 and Glu56 move toward the Cd1 ion in YS29 Cd. Conversely, the Trp26 side chain moves

away from Cd1 as the indole ring rotates. After the conformational change of Trp26, the side chains of Asp52 and Glu56 can be chelated by Cd1.

In summary, the crystal structure of HP-NAP in a zinc or cadmium-bound form reveals the di-nuclear binding mode in which the second ion is more weakly coordinated than the first at the FOC, whereas the iron-containing structure reveals the mononuclear mode. The coordination patterns of Zn^{2+} and Cd^{2+} are different but both metal ions can bind to the FOC, indicating that HP-NAP can store zinc and cadmium ions in addition to iron ions. Another zinc ion is found inside of the negatively-charged three-fold-related pore, as an iron ion in the iron-containing form, and therefore the pore is suitable for metal ions to pass through.

Acknowledgments

We thank Professor R. Nozawa (University of Shizuoka, Japan) for kindly providing the expression vectors for HP-NAP YS29 and YS39. We also thank the Photon Factory staff for assistance with data collection. This study was supported in part by a Grant-in-Aid for Scientific Research (C) (No. 22590039) to S.F. from the Japan Society for the Promotion of Science, and also by a Grant-in-Aid for Young Scientists (B) (No. 21770122) to H.Y. from the Ministry of Education, Culture, Sports, Science and Technology in Japan.

Appendix A. Supplementary data

Supplementary data associated with this article can be found, in the online version, at http://dx.doi.org/10.1016/j.bbrc.2012.05.073.

References

[1] A. Covacci, J.L. Telford, G. Del Giudice, J. Parsonnet, R. Rappuoli, *Helicobacter pylori* virulence and genetic geography, Science 284 (1999) 1328–1333.
[2] C. Montecucco, R. Rappuoli, Living dangerously: how *Helicobacter pylori* survives in the human stomach, Nature Rev. Mol. Cell Biol. 2 (2001) 457–466.
[3] D.J. Evans Jr., D.G. Evans, T. Takemura, H. Nakano, H.C. Lampert, D.Y. Graham, D.N. Granger, P.R. Kvietys, Characterization of a *Helicobacter pylori* neutrophil-activating protein, Infect. Immun. 63 (1995) 2213–2220.
[4] B. Satin, G. Del Giudice, V. Della Bianca, S. Dusi, C. Laudanna, F. Tonello, D. Kelleher, R. Rappuoli, C. Montecucco, F. Rossi, The neutrophil-activating protein (HP-NAP) of *Helicobacter pylori* is a protective antigen and a major virulence factor, J. Exp. Med. 191 (2000) 1467–1476.
[5] S. Kabir, The current status of *Helicobacter pylori* vaccines: a review, Helicobacter 12 (2007) 89–102.
[6] G. Zanotti, E. Papinutto, W.G. Dundon, R. Battistutta, M. Seveso, G. Del Giudice, R. Rappuoli, C. Montecucco, Structure of the neutrophil-activating protein from *Helicobacter pylori*, J. Mol. Biol. 323 (2002) 125–130.
[7] F. Tonello, W.G. Dundon, B. Satin, M. Molinari, G. Tognon, G. Grandi, G. Del Giudice, R. Rappuoli, C. Montecucco, The *Helicobacter pylori* neutrophil-activating protein is an iron-binding protein with dodecameric structure, Mol. Microbiol. 34 (1999) 238–246.
[8] A. Ilari, S. Stefanini, E. Chiancone, D. Tsernoglou, The dodecameric ferritin from *Listeria innocua* contains a novel intersubunit iron-binding site, Nature Struct. Biol. 7 (2000) 38–43.
[9] R.A. Grant, D.J. Filman, S.E. Finkel, R. Kolter, J.M. Hogle, The crystal structure of Dps, a ferritin homolog that binds and protects DNA, Nature Struct. Biol. 5 (1998) 294–303.
[10] P.M. Harrison, P. Arosio, The ferritins: molecular properties, iron storage function and cellular regulation, Biochim. Biophys. Acta 1275 (1996) 161–203.
[11] G. Wang, Y. Hong, A. Olczak, S.E. Maier, R.J. Maier, Dual roles of *Helicobacter pylori* NapA in inducing and combating oxidative stress, Infect. Immun. 74 (2006) 6839–6846.
[12] S.G. Wolf, D. Frenkiel, T. Arad, S.E. Finkel, R. Kolter, A. Minsky, DNA protection by stress-induced biocrystallization, Nature 400 (1999) 83–85.
[13] O. Tsuruta, H. Yokoyama, S. Fujii, A new crystal lattice structure of *Helicobacter pylori* neutrophil-activating protein (HP-NAP), Acta Crystallogr., Sect. F: Struct. Biol. Cryst. Commun. 68 (2012) 134–140.
[14] J.W. Pflugrath, The finer things in X-ray diffraction data collection, Acta Crystallogr., Sect. D: Biol. Crystallogr. 55 (1999) 1718–1725.
[15] Z. Otwinowski, W. Minor, Processing of X-ray diffraction data collected in oscillation mode, Methods Enzymol. 276 (1997) 307–326.
[16] A. Vagin, A. Teplyakov, MOLREP: an automated program for molecular replacement, J. Appl. Crystallogr. 30 (1997) 1022–1025.
[17] Collaborative Computational Project, Number 4, The CCP4 suite: programs for protein crystallography, Acta Crystallogr., Sect. D: Biol. Crystallogr. 50 (1994) 760–763.
[18] G.N. Murshudov, A.A. Vagin, E.J. Dodson, Refinement of macromolecular structures by the maximum-likelihood method, Acta Crystallogr., Sect. D: Biol. Crystallogr. 53 (1997) 240–255.
[19] P. Emsley, K. Cowtan, Coot: model-building tools for molecular graphics, Acta Crystallogr., Sect. D: Biol. Crystallogr. 60 (2004) 2126–2132.
[20] S.C. Lovell, I.W. Davis, W.B. Arendall III, P.I.W. de Bakker, J.M. Word, M.G. Prisant, J.S. Richardson, D.C. Richardson, Structure validation by Cα geometry: φ, ψ and Cβ deviation, Proteins: Struct., Funct., Genet. 50 (2003) 437–450.
[21] E. Krissinel, K. Henrick, Secondary-structure matching (SSM), a new tool for fast protein structure alignment in three dimensions, Acta Crystallogr., Sect. D: Biol. Crystallogr. 60 (2004) 2256–2268.
[22] T. Miyamoto, Y. Asahina, S. Miyazaki, H. Shimizu, U. Ohto, S. Noguchi, Y. Satow, Structures of the SEp22 dodecamer a Dps-like protein from *Salmonella enterica* subsp. *enterica* serovar Enteritidis, Acta Crystallogr., Sect. F: Struct. Biol. Cryst. Commun. 67 (2011) 17–22.
[23] J. Dundas, Z. Ouyang, J. Tseng, A. Binkowski, Y. Turpaz, J. Liang, CASTp: computed atlas of surface topography of proteins with structural and topographical mapping of functionally annotated residues, Nucleic Acids Res. 34 (2006) W116–W118.
[24] L. Rulíšek, J. Vondrášek, Coordination geometries of selected transition metal ions (Co^{2+}, Ni^{2+}, Cu^{2+}, Zn^{2+}, Cd^{2+}, and Hg^{2+}) in metalloproteins, J. Inorg. Biochem. 71 (1998) 115–127.
[25] M.M. Benning, H. Shim, F.M. Raushel, H.M. Holden, High resolution X-ray structures of different metal-substituted forms of phosphotriesterase from *Pseudomonas diminuta*, Biochemistry 40 (2001) 2712–2722.
[26] B. Ren, G. Tibbelin, T. Kajino, O. Asami, R. Ladenstein, The multi-layered structure of Dps with a novel di-nuclear ferroxidase center, J. Mol. Biol. 329 (2003) 467–477.
[27] T. Haikarainen, C.C. Tsou, J.J. Wu, A.C. Papageorgiou, Structural characterization and biological implications of di-zinc binding in the ferroxidase center of *Streptococcus pyogenes* Dpr, Biochem. Biophys. Res. Commun. 398 (2010) 361–365.
[28] T. Haikarainen, A.C. Papageorgiou, Dps-like proteins: structural and functional insights into a versatile protein family, Cell. Mol. Life Sci. 67 (2010) 341–351.
[29] H. Havukainen, S. Haataja, A. Kauko, A.T. Pulliainen, A. Salminen, T. Haikarainen, J. Finne, A.C. Papageorgiou, Structural basis of the zinc- and terbium-mediated inhibition of ferroxidase activity in Dps ferritin-like proteins, Protein Sci. 17 (2008) 1513–1521.